Effect of electron-electron scattering on hot-electron repopulation in n-Si at 77 K*

James G. Nash† and James W. Holm-Kennedy
Electrical Sciences and Engineering Department, School of Engineering and Applied Science, University of California, Los Angeles 90024
(Received 30 October 1975; revised manuscript received 26 July 1976)

Conductivity versus electric field measurements made on $\langle 111 \rangle$ and $\langle 100 \rangle$ crystallographically oriented samples of n-Si at 77 K, with resistivities ranging from 0.049 to 214 Ωcm, are presented and analyzed to determine the effects of electron-electron (e-e) scattering on high-field transport properties. The analysis is based on a theoretical calculation of the high-field electron momentum distribution function, using an iterative technique which allows "exact" solution to difficult nonequilibrium hot-electron problems. The decrease in the $\langle 111 \rangle$ to $\langle 100 \rangle$ conductivity ratio with increasing concentration, caused by the corresponding reduction in valley repopulation, is found to be primarily attributable to intervalley and intravalley e-e scattering. The substantial disagreement between theory and experiment which remains is attributed to ionized or neutral intervalley impurity scattering. Neutral-impurity scattering is also shown to contribute to the repopulation reduction at 600 V/cm, although ionized-impurity scattering had negligible effect at this field. The field and concentration dependence of $\langle 100 \rangle$ repopulation was deduced by a phenomenological scale change technique. The results are consistent with the theoretical calculation. The role of e-e and impurity scattering on the nonequilibrium electron distribution function f is investigated by examining the concentration dependence of f at 600 V/cm. It was found that the isotropic part of f is still non-Maxwellian at a concentration as high as 2×10^{16} cm^{-3} and a field of 1200 V/cm. Experimental results exhibited an apparent increase in free-electron concentration with field. It is estimated that for 1.87-Ωcm material at fields of 1000 V/cm, electron concentration is approximately 30% greater than its thermal-equilibrium value.

I. INTRODUCTION

The role played by electron-electron (e-e) scattering on charge-carrier transport in semiconductors, under the highly nonequilibrium conditions created by large applied electric fields, has received little attention in past years. In this paper, a comprehensive study of its effects on transport in n-Si at 77 K is presented by comparing the field and concentration dependence of the theoretical and experimental-conductivity ratio $\sigma_{\langle 111\rangle}/\sigma_{\langle 100\rangle}$, where $\langle 111\rangle$ and $\langle 100\rangle$ refer to the crystallographic orientation of the field $\vec{E}$.[1] Theoretical calculations were performed using a numerical iterative technique[2] which provides an exact solution to the Boltzmann-transport equation.

It has been previously demonstrated that $\sigma_{\langle 111\rangle}/\sigma_{\langle 100\rangle}$ is a strong function of $\vec{E}$ through the considerable degree of repopulation (redistribution of electrons between "hot" and "cold" sets of energy minima or "valleys" for $\langle 100\rangle$ field applications) that takes place.[3] Repopulation can also be expected to be a strong function of electron concentration n_0. This should occur because of the ability of e-e scattering to modify the energy dependence of the distribution function f (e-e scattering does not affect average drift velocity directly because momentum is conserved in such a collision). If n_0 becomes large enough for the rate of energy exchange between electrons in the same valley, and between electrons in different valleys, to greatly exceed that between electrons and phonons, the isotropic part of the distribution function f_0 in both the hot and cold sets of valleys will become approximately Maxwellian in form with identical electron temperatures or

$$f_0(\epsilon) \propto e^{-\epsilon/k_0 T_e} \ .$$

Here, ϵ is the electron energy, k_0 is Boltzmann's constant, and T_e is the electron temperature. Since f_0 is the same in each valley, no repopulation can occur. Thus, repopulation (and $\sigma_{\langle 111\rangle}/\sigma_{\langle 100\rangle}$) will be large or small depending upon the magnitude of n_0 or the strength of the e-e interaction. We will use this sensitivity of repopulation to concentration to investigate the effects of e-e scattering in a hot-electron environment.

This study will also provide the opportunity to compare the experimentally deduced repopulation and the phenomenological-energy relaxation time with their theoretical counterparts, and to investigate the effects of e-e and impurity scattering on f. Information on the concentration dependence of f can be useful in determining the conditions under which analytical approximations can be used to simplify solution to the Boltzmann-transport equation.

II. LITERATURE REVIEW

There has been little prior study of e-e scattering in n-Si under high-field conditions. This has been due primarily to the mathematical complexity it has introduced when included in a transport

analysis. As a result, many analyses have included the e-e interaction implicitly by assuming a Maxwellian or drifted-Maxwellian form; however, such approximations might lead to large errors, unless the electron concentration is very large.

Experimentally, sensitivity to e-e scattering under high-field conditions has been obtained by examining the concentration dependence of either $\sigma_{\langle 111\rangle}(E)/\sigma_{\langle 100\rangle}(E)$,[4] the phenomenological energy relaxation time τ_ϵ,[5] or the nonlinearity coefficient β,[6] defined by the relation

$$\sigma(E_{\langle 111\rangle}) = \sigma(0)(1+\beta E^2_{\langle 111\rangle}) \ . \tag{1}$$

Although β is reasonably sensitive to e-e scattering, it is only applicable to very low $\langle 111\rangle$ fields where the amount of heating is small and Eq. (1) is applicable. Thus, it does not separate the effects of inter- and intravalley e-e scattering, nor does it describe the effects of e-e scattering on a highly nonequilibrium distribution appropriate to high fields. Similar remarks apply to the usefulness of τ_ϵ. The high-field conductivity ratio, however, suffers neither of these deficiencies, and, in addition, is more sensitive to concentration (it directly reflects repopulation).

Detailed conductivity (or current density) versus $\langle 100\rangle$ and $\langle 111\rangle$ field measurements in n-Si, made using high-voltage pulsed techniques or time-of-flight techniques, have been reported by many authors. However, most of the measurements at 77 K were made for a single resistivity[7-12]; only those of Asche, Boichenko, Bondar, and Sarbei[4] covered a wide range of resistivities. They reported, based on an analysis of two resistivities (1.0 and 0.3 Ω cm), that e-e scattering was primarily responsible for the decrease in repopulation with increasing concentration. However, their theoretical analysis used a Maxwellian approximation for f, and thus was only semiquantitative. Such an approximation also does not allow effects that result from the non-Maxwellian form of f to be included, e.g., intravalley e-e scattering. Our calculation of f shows that intravalley e-e scattering is important and that a Maxwellian f is not achieved for 1.0 and 0.3 Ω cm material at 77 K and fields greater than 200 V/cm.

Repopulation versus $\langle 100\rangle$ electric field in n-Si at 77 K, determined using the scale-change technique has been reported for 6,[13] 10,[14] 15,[13] 23,[7] 26 Ω cm,[8] and high-resistivity (greater than 48 KΩ cm) material.[12] The variation of repopulation with magnetic field at 77 K has been investigated by Heinrich and Kreichbaum in 5 Ω cm material,[10] and the variation with lattice temperature (8–300 K) for very high resistivity material (greater than 48 Ω cm) has been determined by Canali *et al.*[12] We will present here what we believe is the first systematic determination of the concentration dependence of repopulation at 77 K.

III. SAMPLE PREPARATION AND MEASUREMENT TECHNIQUE

The silicon used for the preparation of all samples was obtained in the form of $\langle 111\rangle$ grown ingots doped with phosphorous. Float-zoned silicon was used for resistivities greater than 15 Ω cm to ensure uniformity in doping profile and purity. All other silicon used was Czochralski grown. Recombination lifetimes for the float-zoned material, quoted by the supplier, were several milliseconds. Etch-pit densities for all ingots were quoted as less than 500 cm^{-2}. Thus, the silicon used was relatively free of deep-level impurities and defects.

Samples with resistivities ρ greater than 5 Ω cm were prepared in the same manner as described previously.[3] Those with $\rho < 5$ Ω cm were made with cross sections 250×250 μm^2 in area and 1 cm in length using an ultrasonic cutter. For these samples thermocompression gold bonds were made directly to the n^+ layer.

A summary of sample-doping concentrations and resistivities at 300 and 77 K is given in Table I. The doping concentrations were taken from the work of Irvin[15] who compiled resistivity versus doping results at 300 K from a number of references.

It will be assumed that all our silicon material is uncompensated, i.e., the acceptor concentration is zero. A large degree of compensation is most likely encountered in high-resistivity material. However, as long as doping is uniform, compensation is not important because such few impurities will not play a role in transport. Since little variation in resistivity was found from sample to sample in that resistivity range, this is good evidence that there was no doping inhomogeneity.

The free-electron concentration n_0 (Table I) was obtained by solving the charge-balance equation for the Fermi level. The ground state energy of phosphorus was assumed to be 43.5 meV below the conduction band[16] and excited state energies were taken from Kohn and Luttinger[17] and Long and Meyers.[18] Determination of n_0 this way gave good agreement between experimental and theoretical resistivity versus temperature from 77 to 300 K for all but the most heavily doped specimen (0.049 Ω cm). For very heavily doped material the effective-donor ionization energy decreases due to adjacent-donor wave-function overlap.

Current density versus electric field measurements were made using a high-voltage dc pulse technique described earlier.[3]

TABLE I. Measured sample resistivities and doping concentrations.

300 K $\rho\langle 111\rangle$(Ω cm)	300 K $\rho\langle 100\rangle$(Ω cm)	300 K $\rho\langle 110\rangle$(Ω cm)	77 K $\rho\langle 111\rangle$(Ω cm)	77 K $\rho\langle 100\rangle$(Ω cm)	77 K $\rho\langle 110\rangle$(Ω cm)	N_a(cm^{-3})$\langle 111\rangle$	77 K n_0(cm^{-3})$\langle 111\rangle$
214.0	220.0	212.0	14.5	14.9	14.4	2.30×10^{13}	2.25×10^{13}
152.0	151.0	154.0	10.1	9.83	9.90	3.25×10^{13}	3.16×10^{13}
57.7	57.6	57.6	4.11	4.04	4.00	8.90×10^{13}	8.31×10^{13}
50.0	51.0	48.6	3.63	3.68	3.62	1.00×10^{14}	9.24×10^{13}
14.8	14.4	13.9	1.40	1.31	1.32	3.15×10^{14}	2.58×10^{14}
7.66	7.88	7.71	0.955	0.962	0.969	6.20×10^{14}	4.48×10^{14}
3.56	3.35	•••	0.551	0.539	•••	1.40×10^{15}	8.22×10^{14}
1.87	1.82	•••	0.389	0.396	•••	2.65×10^{15}	1.27×10^{15}
0.367	0.367	•••	0.173	0.167	•••	1.70×10^{16}	3.91×10^{15}
0.0490	0.0517	•••	0.122	0.128	•••	2.00×10^{17}	$\sim2.3\times10^{16}$

IV. EXPERIMENTAL RESULTS

The conductivity ratio $(\sigma_{\langle 111\rangle}/\sigma_{\langle 100\rangle})$ vs $\vec{E}$ measurements for the resistivities in Table I are shown in Fig. 1.[19] A field range from 0 to 2000–3000 V/cm was generally sufficient to include most of the conductivity anisotropy. Because intervalley phonon-induced repopulation is associated with an increased number of electrons in the low-mobility cold valleys and a decreased number of electrons in the high-mobility hot valleys, $\sigma_{\langle 100\rangle}$ will always be less than $\sigma_{\langle 111\rangle}$, for which no repopulation occurs. The conductivity ratio, which reflects the degree of repopulation, begins to decrease at a concentration of about 3×10^{13} cm^{-3} (152 Ω cm). This is attributed at least in part to the predicted thermal-shorting effect between hot and cold valleys caused by the increased e-e scattering with increased concentration. One notices that the repopulation peak shifts toward higher fields with increasing concentration. We believe this is due to the suppression of carrier heating which occurs when the increased impurity scattering reduces the mobility. At fields greater than 1500 V/cm the conductivity curves tend to converge. This is expected, since for strong-carrier heating, impurity and e-e scattering become weak compared to lattice scattering. Repopulation is then only dependent on lattice scattering which is the same for all samples, regardless of concentration.

The conductivity ratio $(\sigma_{\langle 111\rangle}/\sigma_{\langle 110\rangle})$ vs $\vec{E}$ (Fig. 2) shows the same general characteristics as in Fig. 1, except that it is much smaller. (For a ⟨110⟩ field there are four thermally equivalent hot valleys and two cold valleys.) This is to be expected because the relative heating of electrons in hot and cold valleys is much less. No anisotropy in the conductivity ratio was observable at room temperature up to fields of 4000 V/cm.

To check the consistency and reproducibility of the experiment, $(\sigma_{\langle 111\rangle}/\sigma_{\langle 100\rangle})$ vs $\vec{E}$ curves, obtained from samples cut from two different silicon ingots of approximately the same resistivity (50.0 and 57.7 Ω cm, Table I) were compared. Agreement was better than ± 2% for fields up to 1500 V/cm.

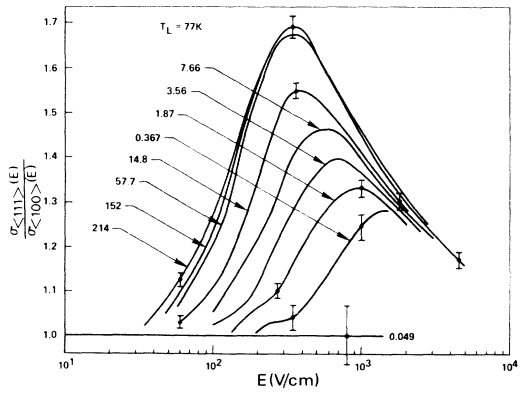

FIG. 1. Experimental ⟨111⟩ to ⟨100⟩ conductivity ratio vs field for various resistivities (given in units of Ω cm).

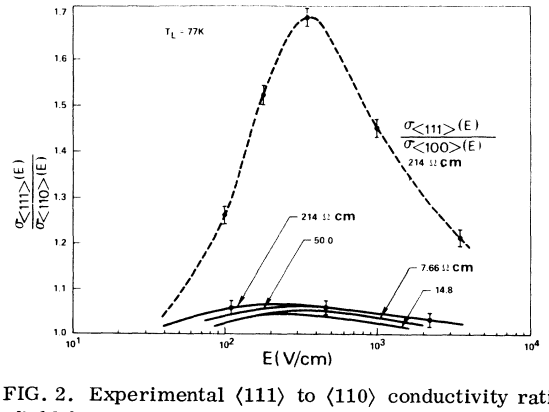

FIG. 2. Experimental ⟨111⟩ to ⟨110⟩ conductivity ratio vs field for various resistivities. The 214-Ω cm ⟨111⟩ to ⟨100⟩ conductivity ratio is included for comparison.

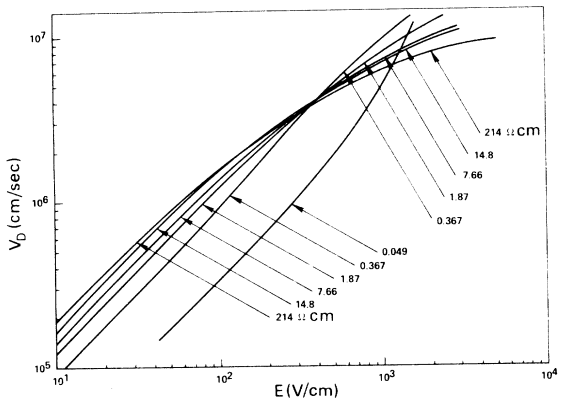

FIG. 3. Inferred drift velocity vs ⟨111⟩ field obtained from current density measurements.

Drift velocity v_D vs ⟨111⟩ field can be obtained by dividing $J_{\langle 111\rangle}(E)$ by the factor $n_0 e$, assuming n_0 is not a function of field. These results are shown in Fig. 3 for a wide range of resistivities.

Repopulation for ⟨100⟩ fields can be determined by writing $J_{\langle 100\rangle}$ and $J_{\langle 111\rangle}$ in terms of valley mobilities and concentrations as follows[8]:

$$J_{\langle 100\rangle} = e(4n_\perp \mu_\perp + 2n_{\parallel}\,\mu_{\parallel})E_{\langle 100\rangle} \tag{2}$$

and

$$J_{\langle 111\rangle} = e n_0\, \mu_{\langle 111\rangle} E_{\langle 111\rangle}\ , \tag{3}$$

where $n_\perp$, $\mu_\perp$ and $n_{\parallel}$, $\mu_{\parallel}$ are the concentrations and mobilities in the hot and cold valleys, and $\mu_{\langle 111\rangle}$ is the mobility in all valleys for a ⟨111⟩ field. The field dependence of mobilities and concentrations (except n_0) is implicitly assumed. Using carrier conservation

$$4n_\perp + 2n_{\parallel} = n_0\ ,$$

Eqs. (2) and (3) can be solved to give

$$n_\perp(E) = \frac{n_0}{4}\left(\frac{[J_{\langle 100\rangle}(E)/J_{\langle 111\rangle}(E)]\,\mu_{\langle 111\rangle} - \mu_{\parallel}}{\mu_\perp - \mu_{\parallel}}\right) \tag{4}$$

and

$$n_{\parallel} = \tfrac{1}{2} n_0 - 2n_\perp(E)\,. \tag{5}$$

In Eq. (4), $J_{\langle 100\rangle}$, $J_{\langle 111\rangle}$, and $\mu_{\langle 111\rangle}$ are known from the experimental results; however, $\mu_{\parallel}$ and $\mu_\perp$ cannot be measured directly. These can be determined from considerations based on the use of the energy balance equation

$$-\left\langle\frac{d\epsilon}{dt}\right\rangle\Big|_{\text{scattering}} = \left\langle\frac{d\epsilon}{dt}\right\rangle\Big|_{\text{fields}}\ , \tag{6}$$

which equates average energy losses due to scattering with average energy gain from the field in a single valley. The field term is $e\vec{E}\cdot\underline{\mu}\cdot\vec{E}$ and the scattering term is modeled phenomenologically as

$$\left\langle\frac{d\epsilon}{dt}\right\rangle\Big|_{\text{scattering}} = -\,\frac{\bar{\epsilon} - \frac{3}{2}k_0 T_L}{\tau_\epsilon(\bar{\epsilon})}\ ,$$

where $\bar{\epsilon}$ is the average energy, τ_ϵ is a "phenomenological energy relaxation time" characterizing the rate of electron energy loss to scattering mechanisms, and T_L is the lattice temperature. (e-e scattering will be ignored for the present, restricting the results to lightly doped material.) Therefore, Eq. (6) can be rewritten

$$(\bar{\epsilon} - \tfrac{3}{2}k_0 T_L)/\tau_\epsilon(\bar{\epsilon}) = e\,\mu_\theta E^2\ , \tag{7}$$

where

$$\mu_\theta = \mu_{\parallel}\cos^2\theta + \mu_\perp \sin^2\theta$$

and θ is the angle between $\vec{E}$ and the major axis of the valley. For a fixed ⟨111⟩ field E_β, Eq. (7) becomes

$$(\bar{\epsilon}_\beta - \tfrac{3}{2}k_0 T_L)/\tau_\epsilon(\bar{\epsilon}_\beta) = e[\mu_{\parallel}(\bar{\epsilon}_\beta)\cos^2\beta + \mu_\perp(\bar{\epsilon}_\beta)\sin^2\beta]E_\beta^2\ , \tag{8}$$

where $\beta = 54°\ 44'$ and it has been assumed that mobilities can be written as a function of average energy $\bar{\epsilon}_\beta$.[8] By equating the right-hand sides of Eqs. (7) and (8), the magnitude of the field E_θ, applied at an arbitrary angle θ, that gives the same average energy $\bar{\epsilon}_\beta$, can be determined. This field is

$$E_\theta^2 = \lambda_\theta^2 E_\beta^2\ , \tag{9}$$

where

$$\lambda_\theta = \left(\frac{\cos^2\beta + (m_{\parallel}/m_\perp)\sin^2\beta}{\cos^2\theta + (m_{\parallel}/m_\perp)\sin^2\theta}\right)^{1/2}\ . \tag{10}$$

Equation (10) shows that $\lambda_{90} = 0.86$ and $\lambda_0 = 1.94$. Since the normalized mobility $\mu_{\langle 111\rangle}(E_\beta)/\mu_{\langle 111\rangle}(0)$ is known from experiment, the normalized mobility $\mu_\theta(E_\theta)/\mu_\theta(0)$ for an arbitrary θ can be found using the scale factor λ_θ. This is true because the mobility has been assumed to be a function of average energy, and thus, μ_θ can be obtained from $\mu_{\langle 111\rangle}$ by finding the field E_θ which gives the same average energy as a particular value of ⟨111⟩ field. Mathematically, this means that

$$\frac{\mu_\theta(E_\theta)}{\mu_\theta(0)} = \frac{\mu_\theta(E_\beta\lambda_\theta)}{\mu_\theta(0)} = \frac{\mu_{\langle 111\rangle}(E_\beta)}{\mu_{\langle 111\rangle}(0)}\ . \tag{11}$$

Noting the definitions

$$\mu_{\parallel}(E) \equiv \mu_0(E_0)$$

and

$$\mu_\perp(E) \equiv \mu_{90}(E_{90})\ ,$$

and using Eq. (11), Eq. (4) can be rewritten

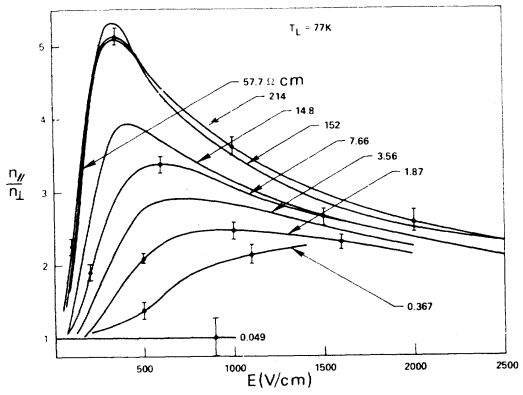

FIG. 4. Experimentally deduced ratio of free-electron concentration in a cold valley ($n_{\parallel}$) to that in a hot valley ($n_\perp$) vs ⟨100⟩ field for various resistivities.

$$n_\perp = \frac{n_0}{4}\,\frac{\lambda_0^2\sigma_{\langle 100\rangle}(E)/\sigma_{\langle 111\rangle}(E/\lambda_0) - 1}{\lambda_0^2\sigma_{\langle 111\rangle}(E/\lambda_{90})/\lambda_{90}^2\sigma_{\langle 111\rangle}(E/\lambda_0) - 1}\,. \tag{12}$$

Because $n_\perp$ is not determined directly from experiment, it is termed "experimentally deduced." Kastner *et al.*[7] and Nougier *et al.*[13] have also independently given formulations for deducing repopulation in silicon. Their formalism can be shown to be identical to that in Eq. (12) by noting that

$$\lambda_0^2 = \tfrac{1}{3}(1 + 2m_{\parallel}/m_\perp)$$

and

$$\lambda_{90}^2 = \frac{1 + 2m_{\parallel}/m_\perp}{3m_{\parallel}/m_\perp}\,.$$

Substitution of these two expressions in Eq. (12) yields expressions in exact correspondence to those of Kastner *et al.* and Nougier *et al.*

Repopulation for ⟨100⟩ fields, calculated from Eq. (12) is shown in Fig. 4.[20] These curves exhibit the same general characteristics as shown by the conductivity ratio in Fig. 1. Repopulation, calculated for a ⟨110⟩ field (Fig. 5) is much smaller than for a ⟨100⟩ field.

The repopulation analysis has been based upon the use of a scale factor λ_θ, which enabled the terms $\mu_\perp(E)$ and $\mu_{\parallel}(E)$ in Eq. (4) to be determined. An important assumption implicit in the derivation of Eq. (12), was that the valleys were thermally isolated.[8] This allowed the energy-balance relationship [Eq. (7)], from which λ_θ was derived, to be written down independently for each valley. The assumption of thermal isolation between valleys cannot be valid for strong *e-e* scattering. However, the ensuing analysis will show that this lack of thermal isolation still does not invalidate the use of the scale change technique in deducing repopulation.

The effect of *e-e* scattering on the energy balance relationship can be characterized phenomenologically by

$$\left\langle \frac{d\epsilon}{dt} \right\rangle\Bigg|_{e\text{-}e} = -\,\frac{\bar{\epsilon}_1 - \bar{\epsilon}_2}{\tau_{ee}(\bar{\epsilon}_1, \bar{\epsilon}_2, n_1, n_2)}\,, \tag{13}$$

which gives the average rate of energy loss in a hot valley. Here, $\bar{\epsilon}_i$ and n_i are the average energy and concentration in the hot ($i = 1$) and cold ($i = 2$) valleys, and τ_{ee} is a relaxation time which describes the rate of energy exchange between them. For a ⟨100⟩ field orientation, the energy-balance equation [Eq. (7)] for a hot valley ($\theta = 90$) becomes, after addition of the *e-e* term [Eq. (13)]

$$\frac{\bar{\epsilon}_1 - \frac{3}{2}k_0T_L}{\tau_\epsilon(\bar{\epsilon}_1)} = -\,\frac{\bar{\epsilon}_1 - \bar{\epsilon}_2}{\tau_{ee}(\bar{\epsilon}_1, \bar{\epsilon}_2, n_1, n_2)} + e\mu_\perp(\bar{\epsilon}_1)E_{90}^2\,. \tag{14}$$

For a ⟨111⟩ field orientation the energy balance relationship for the same valley is

$$\frac{\bar{\epsilon}_\beta - \frac{3}{2}k_0T_L}{\tau_\epsilon(\bar{\epsilon}_\beta)} = e\mu_{\langle 111\rangle}(\bar{\epsilon}_\beta)E_\beta^2\,. \tag{15}$$

Equation (15) does not include an *e-e* term because all valleys are heated equally and thus there can be no net energy exchange between valleys due to this mechanism. For the hot valley, the scale-change technique requires the field E_{90} such that $\bar{\epsilon}_1 = \bar{\epsilon}_\beta$. This field is found by equating the right-hand sides of Eqs. (14) and (15) and solving for E_{90}. The result is

$$E_{90}^2 = \lambda_{90}^2 E_{\langle 111\rangle}^2 + (\bar{\epsilon}_1 - \bar{\epsilon}_2)/\tau_{ee}\mu_\perp(\bar{\epsilon}_1)\,. \tag{16}$$

Equation (16) states that the field E_{90} required for $\bar{\epsilon}_1 = \bar{\epsilon}_\beta$ is greater than would be the case for

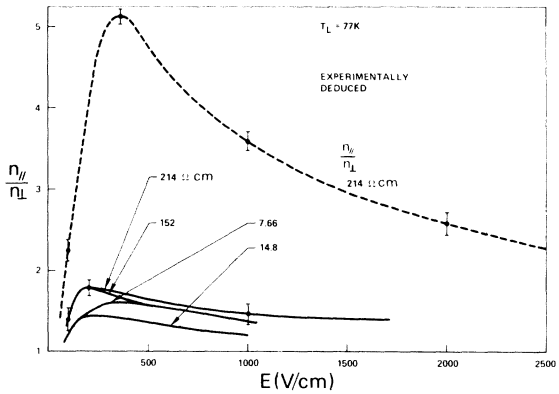

FIG. 5. Experimentally deduced ratio of free-electron concentration in a cold valley (n_{45}) to that in a hot valley (n_{90}) vs ⟨110⟩ field for various resistivities. The ⟨100⟩ repopulation curve for 214 Ω cm is shown for comparison.

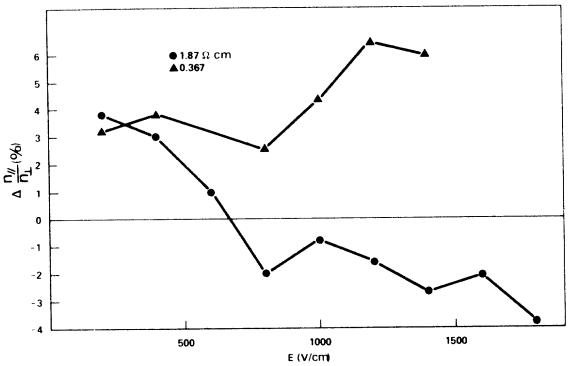

FIG. 6. Percent change in experimentally deduced ⟨100⟩ repopulation (Fig. 4) when recalculated using a scale factor equal to 1.

no e-e scattering ($\tau_{ee} \to \infty$). This is to be expected on physical grounds, because the hot valley loses additional energy to the cold valleys via intervalley e-e scattering, which it otherwise would not lose if there were no e-e scattering ($\tau_{ee} \to \infty$). Therefore, an even higher field E_{90} is needed to satisfy the requirement $\bar{\epsilon}_1 = \bar{\epsilon}_\beta$. This means that the appropriate scale factor relating E_{90} to E_β would have to be larger than $\lambda_{90}(0.86)$, the low-concentration limit of the scale factor. This scale factor would also increase in magnitude with increasing concentration due to the greater amount of intervalley e-e energy exchange between valleys. Its upper limit would necessarily be one, because for very high concentrations energy exchange between valleys would be strong enough to keep all valleys at the same average energy, regardless of field orientation. In other words $\bar{\epsilon}_1 = \bar{\epsilon}_\beta$ even when $E_{90} = E_\beta$. In a similar manner, it can be established that the appropriate scale factor for a cold valley will decrease from $\lambda_0(1.96)$ with increasing concentration, reaching one in the limit of large concentrations.

To test the effect of a variation in scale factor with concentration, the ⟨100⟩ repopulation was recalculated using Eq. (12), with a scale factor equal to one ($\lambda_\theta = 1$), the high-concentration limiting value. The resulting percent change in repopulation from that calculated using $\lambda_{90} = 0.86$ and $\lambda_0 = 1.96$ (Fig. 4) is shown in Fig. 6 for two higher-concentration samples (where the error is expected to be worst in Fig. 4). The maximum error over a wide-field range is only 6%. Since this high-concentration limit ($\lambda_\theta = 1$) is not reached for any resistivity in Fig. 4, except 0.049 Ω cm, one expects that neglect of e-e scattering in Eq. (12) will lead to little error.

The lack of sensitivity of the repopulation formula [Eq. (12)] to the effects of intervalley e-e scattering is not fortuitous, but is a consequence of the magnitude of repopulation-induced anisotropy. By allowing scale factors to equal one (equivalent to setting $m_\parallel = m_\perp$), repopulation is calculated based on the assumption that field orientation does not alter the average energy of a valley, i.e., all valleys are treated as if they were heated equally. In this manner, only anisotropy arising from repopulation is included in the calculations. However, since repopulation-induced anisotropy is much larger than mobility anisotropy, this is a good approximation. To illustrate the difference between repopulation- and mobility-induced anisotropy in current density, Fig. 7 shows measured 214 Ω cm $J_{\langle 100\rangle}$ and $J_{\langle 111\rangle}$ versus $\vec{E}$. Also shown is a "hypothetical" ⟨100⟩ curve, calculated assuming there is no repopulation anisotropy ($n_\parallel / n_\perp = 1$), but allowing mobility anisotropy. It is evident that anisotropy due to mobility is indeed small.

V. CALCULATION OF THE DISTRIBUTION FUNCTION

A. Introduction

The formulation for determining the distribution function is based on an "exact" iterative technique[21] described in Ref. 3. There, intervalley phonon, acoustic phonon, and ionized impurity-scattering mechanisms were included. In this study, neutral impurity and e-e scattering need also be included. The collision terms for these two scattering mechanisms are described in the following paragraphs.

In this analysis, lattice-scattering parameters and other constants have been taken from Table I in Ref. 3. Also, for 0.049 Ω cm material, ionized

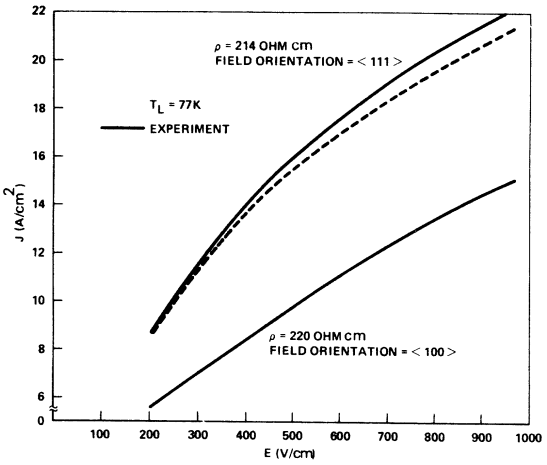

FIG. 7. Experimental ⟨111⟩ and ⟨100⟩ current density vs field (solid lines) and hypothetical ⟨100⟩ current density vs field calculated assuming no repopulation (dashed line).

impurity scattering has been neglected at very-low-electron energies in order to achieve numerical convergence in a reasonable time span. The effect of ionized impurity scattering is to reduce the anisotropy in $f(\vec{u})$ ($\vec{u}$ is a transformed wave vector described in Ref. 3); however, since $f(\vec{u})$ is nearly isotropic at low energies even in the absence of ionized impurity scattering, this neglect should not be important.

B. Electron-electron scattering

In order to characterize the interaction of electrons among themselves, it is helpful to look at some important physically descriptive parameters. These are d, the mean distance of an electron to its nearest neighbor; b_0, the value of the collision or impact parameter (the distance of closest approach between two electrons in the absence of any mutual force) for which an electron is deflected 90° in a collision with another electron, and λ_D is the Debye shielding distance. For an electron gas having an average energy $\frac{3}{2}k_0T_e$, the parameters are

$$b_0 = e^2/3\kappa k_0 T_e \ ,$$

$$d = n_0^{-1/3} \ ,$$

and

$$\lambda_D = (\kappa k_0 T_e/4\pi n_0 e^2)^{1/2} \ ,$$

where κ is the dielectric constant. These parameters, calculated for various values of n_0 with $T_e = 200$ K (Table II), show that the relation

$$b_0 < d < \lambda_D$$

holds over almost three orders of magnitude of concentration variation (10^{13}–10^{16} cm^{-3}). If the impact parameter b for a particular collision satisfies $b < d$, then an electron can interact with only one other electron at a time and thus collisions can be adequately described in terms of successive two-body or binary encounters. If $b_0 < b < d$, collisions are still binary, but small angle. If $d < b < \lambda_D$ collisions are still small angle but can no longer be considered binary, since several collisions will be taking place at the same time. For $\lambda_D < b$ there will be no scattering because sufficient screening exists between electrons to prevent their interaction. The degree to which small-angle scattering ($b_0 < b$) dominates over large-angle scattering ($b < b_0$) can be determined by comparing the time t_m for a 90° deflection of an electron resulting from a number of multiple weak scatters, and the time t_1 for a 90° deflection due to a single scatter. This ratio (t_1/t_m) is given by 8 ln (λ_D/b_0),[22] which from Table II is seen to be quite large over the concentration range 10^{13}–10^{16} cm^{-3}.

TABLE II. Constants describing electron-electron scattering calculated for $T_e = 200$ K.

		n_0 (cm^{-3})			
		10^{13}	10^{14}	10^{15}	10^{16}
10^{-6} cm	b_0	0.23	0.23	0.23	0.23
	d	46	22	10	4.6
	D	110	34	11	3.4
	$8\ln(\lambda_D/b_0)$	49	39	30	21

In this analysis a Fokker-Planck formulation of the e-e collision term[22]

$$\left(\frac{\partial f^{(i)}}{\partial t}\right)_{ee} = -\sum_j \{2A\vec{\nabla}\cdot[f^{(i)}(\vec{v})\vec{\nabla}S^{(j)}(\vec{v})] + \tfrac{1}{2}\vec{\nabla}\vec{\nabla}:[f^{(i)}(\vec{v})\vec{\nabla}\vec{\nabla}T^{(j)}(\vec{v})]\} \qquad (17)$$

is used. Here

$$S^{(j)}(\vec{v}) = 2\int \frac{f^{(j)}(\vec{v}')}{|\vec{v}-\vec{v}'|}\, d\vec{v}' \ ,$$

$$T^{(j)}(\vec{v}) = \int f^{(j)}(\vec{v}')\,|\vec{v}-\vec{v}'|\, d\vec{v}' \ ,$$

and

$$A = (4\pi m_d e^4/h^3\kappa^2)\ln(\lambda_D/b_0) \ ,$$

where m_d is the density of states mass, h is Planck's constant, and $f^{(i)}$ correspond to the distribution functions in the hot ($i = 1$) and cold ($i = 2$) sets of valleys. The gradients are all with respect to velocity (spherical energy surfaces are assumed). Equation (17) can be derived assuming collisions are small angle and binary ($b_0 < b < d$); however, the same result has been obtained for $d < b < \lambda_D$, where the assumption of binary collisions is no longer valid.[23] Thus, since large-angle scattering ($b < b_0$) is of considerably less importance than small-angle scattering ($b_0 < b$), the Fokker-Planck formulation should be adequate for describing e-e scattering.

The assumption of spherical energy surfaces was necessary because we were not able to easily include e-e scattering between spheroidal thermally nonequivalent valleys in the collision term. As a measure of the error associated with the spherical-valley assumption, we calculated the rate of energy exchange between a hot and cold valley (using a Maxwellian distribution) for two cases, spheroidal and spherical valleys with the same density-of-states mass.[24,25] Since it was found that the two rates were approximately the same, the spherical valley assumption appeared reasonable.

For e-e scattering we only include the zeroth order collision term harmonic $(\partial f_0^{(i)}/\partial t)_{e\text{-}e}$, where

$f_0^{(i)}$ is the first term in a Legendre expansion of the distribution function. (The ellipsoidal energy surfaces have been transformed into spherical energy surfaces.[3]) This is physically reasonable because the principal effect of e-e scattering is expected to be on the energy distribution of electrons, which is determined by $f_0^{(i)}$. The contribution of $f_1^{(i)}$, which determines drift velocity, is expected to be very small because total velocity is conserved in an e-e collision. These conclusions are also consistent with those of Rees,[21] who did not neglect higher order e-e collision terms in his theoretical treatment of transport in GaAs at 77 K. In his iterative calculation, ionized impurity scattering was found to have a much stronger effect on drift velocity than e-e scattering.

In Appendix A, it is shown that Eq. (17) reduces to

$$\left(\frac{\partial f_0^{(i)}}{\partial t}\right) = \frac{A}{\sqrt{2}} \sum_j \left[4\pi f_0^{(i)}(v) f_0^{(j)}(v) + \frac{1}{v^2}\left(\frac{\partial f_0^{(i)}}{\partial v}\right)\left(\frac{\partial T_0^{(j)}}{\partial v}\right) + \frac{1}{2}\left(\frac{\partial^2 f_0^{(i)}}{\partial v^2}\right)\left(\frac{\partial^2 T_0^{(j)}}{\partial v^2}\right)\right], \tag{18}$$

where

$$T_0^{(j)} = \int |\bar{v} - \bar{v}'| f_0^{(j)}(\bar{v}')\, d\bar{v}'.$$

In order to proceed, it is assumed that for the purposes of calculating $T_0^{(j)}$, $f_0^{(j)}$ can be treated as Maxwellian at an electron temperature T_{ej}, determined from the average energy of that valley. This should be a good approximation because the derivatives of $T_0^{(j)}$ in Eq. (18) involve an integral over $f_0^{(j)}$, so that the details in the variation $f_0^{(j)}$ with velocity will be averaged out. Thus, assuming

$$f_0^{(j)} = \sqrt{2}\, n_j \left(\frac{2\pi\hbar^2}{m_d k_0 T_{ej}}\right)^{3/2} e^{-m_d v^2/2k_0 T_{ej}},$$

where n_j is the electron concentration in the jth set of valleys, we have

$$T_0^{(j)}(v) = \frac{4\pi n_j}{x_j}\left(\frac{\hbar}{m_d}\right)^3 \left(\frac{2k_0 T_e}{m_d}\right)^{1/2} \times \left[\sqrt{\pi}\left(\tfrac{1}{2} + x_j^2\right)\operatorname{erf}(x_j) + x_j e^{-x_j^2}\right], \tag{19}$$

where

$$x_j^2 = m_d v^2/2k_0 T_{ej}.$$

In taking the derivatives of $f_0^{(i)}$, the same "local" temperature approximation introduced in Ref. 3 is used. Thus,

$$\frac{\partial f_0^{(i)}}{\partial v} = -\frac{m_d v}{k_0 T_{\text{loc}}^i} f_0^{(i)}(v) \tag{20}$$

and similarly for the second derivative of $f_0^{(i)}$. Using Eqs. (19) and (20), Eq. (18) becomes

$$\left(\frac{\partial f_0^{(i)}(u)}{\partial t}\right) = \frac{4\pi A}{\sqrt{2}} \sum_j f_0^{(i)}(u) \left\{ f_0^{(j)}(u)\left[1 - \left(\frac{T_{ej}}{T_{\text{loc}}^i(u)}\right)^2\right] + \frac{2\sqrt{2}\,\pi^2 n_j \hbar^2}{u m_d k_0 T_{ej}} \operatorname{erf}\left(\frac{\hbar u}{(2m_d k_0 T_{ej})^{1/2}}\right)\left(\frac{T_{ej}}{T_{\text{loc}}^i(u)}\right)^2 \left(1 - \frac{T_{\text{loc}}^{(i)}(u)}{T_{ej}}\right)\right]\right\}, \tag{21}$$

where transformed wave-vector coordinates u are used ($\hbar u = m_d v$, as described in Ref. 3) instead of velocity coordinates. For a system of two gases it is assumed that it is adequate to use

$$b_0 = 2e^2/3k_0(T_{e1} + T_{e2})\kappa.$$

C. Neutral impurity scattering

The Erginsoy formulation of neutral impurity scattering yields an elastic and isotropic momentum-relaxation time[26,27]

$$\tau_m^{\text{neu}} = m_c m_d e^2/20(N_d - n_0)\hbar^3\kappa.$$

where m_c is the conductivity effective mass (given in Table I of Ref. 3). Thus

$$\left(\frac{\partial f_0^{(i)}}{\partial t}\right)_{\text{neu}} = 0$$

(since scattering is elastic) and

$$\left(\frac{\partial f_n^{(i)}}{\partial t}\right)_{\text{neu}} = -\frac{f_n^{(i)}(u)}{\tau_m^{\text{neu}}}. \tag{22}$$

VI. ANALYSIS

In this section, the effect of e-e and impurity scattering (ionized and neutral) on conductivity anisotropy is investigated by comparison of theoretical and experimental $\sigma_{\langle 111\rangle}/\sigma_{\langle 100\rangle}$ ratio for 214, 7.66, 1.87 and 0.049 Ω cm material. This represents a concentration range (2.3×10^{13} to 2×10^{16} cm^{-3}), sufficient to encompass all the variation of repopulation with concentration for fields up to 2000 V/cm. The conductivity ratio is analyzed rather than the $\langle 100\rangle$ conductivity alone, because this ratio is insensitive to small changes in the values of free-electron concentration. This insensitivity is necessary because electron concentration increases slightly with field (Sec. VIII).

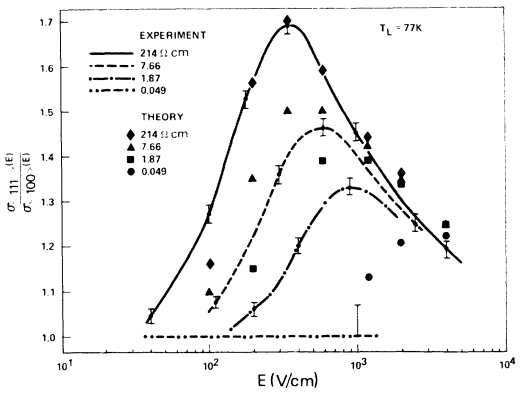

FIG. 8. Theoretical and experimental ratio of ⟨111⟩ to ⟨100⟩ conductivity vs field.

The comparison of experimental and theoretical results for the resistivities mentioned above is made in Fig. 8. The theoretically calculated conductivity ratio decreases, and its peak shifts to higher fields, as concentration is increased. This behavior is consistent with the experimental results, although there remains a fair difference in the relative magnitude of experimental and theoretical curves.

The decrease in the conductivity ratio with increasing concentration, we attribute primarily to e-e scattering. For example, elimination of e-e scattering from the calculation for a ⟨100⟩ field of 600 V/cm (1.87 Ω cm material) showed that approximately 55% of the experimentally seen repopulation reduction was due to e-e scattering. To explain how the e-e interaction can control repopulation, one notes that when impurity and e-e scattering are unimportant, there is a depletion of electron density in the "tail" of the distribution or energies greater than the 680 K f-type phonon energy (see discussion in Ref. 3), when compared to a Maxwellian distribution with the same average energy. Furthermore, the amount of depletion is much greater in the cold than the hot set of valleys, because electrons in the hot set of valleys gain energy from the field more rapidly that those in the cold valleys. This effect is illustrated in Fig. 9, which shows that the ratio of the coefficients $f_0^{(1)}$ and $f_0^{(2)}$, each normalized to the concentration in the hot (1) and cold (2) sets of valleys, is much greater than one in the tail of the distribution. (The coefficient $f_0^{(i)}$ determines the energy dependence of electron concentration.) The principal effect of the e-e interaction is to attempt to constrain $f_0^{(1)}$ and $f_0^{(2)}$ to identical Maxwellian forms. To accomplish this, the e-e interaction must "pump" electrons from lower energies into the depleted tails of $f_0^{(1)}$ and $f_0^{(2)}$. Since the tail of $f_0^{(2)}$ is more depleted than that of $f_0^{(1)}$ (greater deviation from Maxwellian form), the pumping rate into the $f_0^{(2)}$ tail is enhanced relative to that into $f_0^{(1)}$. This in turn decreases repopulation because a greater number of electrons are available for scattering from the cold back to the hot valleys by spontaneous emission of the 680 K phonon (intervalley transfers by phonon absorption are unimportant at 77 K). Thus, e-e scattering controls repopulation through the relative rates at which electrons are pumped into the hot and cold valley tails.

Intervalley and intravalley e-e scattering both perform a similar function, namely, to attempt to bring about a Maxwellian form for $f_0^{(1)}$ and $f_0^{(2)}$.[28] They differ only in that intervalley e-e scattering also produces energy exchange between hot and cold valleys. If only intravalley e-e scattering were present, repopulation would still decrease with increasing n_0, at least up to the value of n_0 where the distribution functions in hot and cold valleys were Maxwellian with different electron temperatures. A further reduction in repopulation would take place with the inclusion of intervalley e-e scattering, because it would constrain $f_0^{(1)}$ and $f_0^{(2)}$ in hot and cold valleys to the same electron temperatures.

To illustrate the roles played by the inter- and intravalley process, we calculate in Fig. 10 the relative contributions they make to the rate at

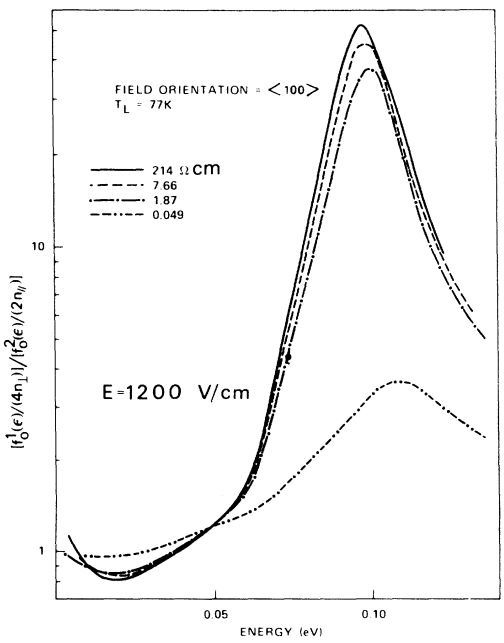

FIG. 9. Ratio of the normalized Legendre coefficients $f_0^{(i)}$ in a hot (i = 1) and cold (i = 2) valley as a function of energy.

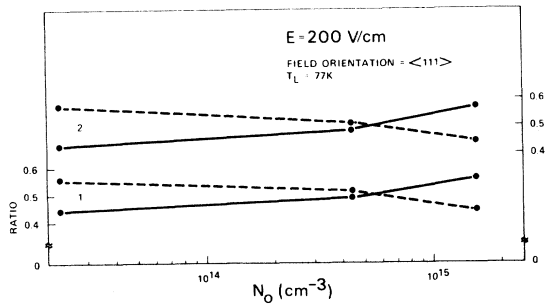

FIG. 10. Electron-flow rates into the distribution tail of a hot valley (1) and cold valley (2) due to electrons in the hot (solid line) and cold (dashed line) sets of valleys as a function of n_0. These rates are normalized to the total flow rates into the hot and cold sets of valleys.

which electrons are "pumped" into the distribution tails in the hot and cold valleys for a ⟨100⟩ field of 200 V/cm. Interestingly, at low values of n_0 (2.3×10^{13} cm^{-3}), electrons in the cold valleys serve as the primary pump of electrons into the distribution tails in all valleys. One might intuitively expect that the hot-valley electrons would perform this function, since they have the larger average energy. The reason that the cold set of valleys is a more effective pump for this field and concentration is that the e-e scattering strength is larger due to the preponderance of electrons in these valleys. However, as n_0 increases, repopulation decreases in magnitude and electrons in the hot set of valleys control the pumping rate. Thus, repopulation is largely responsible for the relative roles played by hot and cold valley electrons on the pumping rates into the distribution tails.

Although the drop in repopulation with increasing concentration is primarily attributable to e-e scattering, there is a contribution to this drop from impurity scattering. For example, at a ⟨100⟩ field of 600 V/cm in 1.87 Ω cm material, it was found that roughly 25% of the experimentally seen drop in repopulation was due to neutral impurity scattering. To explain this, we note that the tails of $f_0^{(1)}$ and $f_0^{(2)}$ are streamed in the field direction at 600 V/cm for high-resistivity material.[3] Since neutral impurity scattering is isotropic, electrons at a particular energy in the tails of $f_0^{(1)}$ and $f_0^{(2)}$, moving in the field direction, will tend (with increasing neutral impurity scattering) to be scattered to the same energy, moving opposite to the field direction, thereby reducing the degree of streaming. However, electrons moving opposite to the field direction are rapidly decelerated out of the tails of $f_0^{(1)}$ and $f_0^{(2)}$ to lower energies. In this manner, impurity scattering works to pump electrons out of the distribution tail. Since the hot valley is more streamed than the cold valley (the transformed field is higher there), this pumping rate will be greater out of its tail; thus, repopulation is reduced because the relative number of electrons available for scattering from the hot to the cold set of valleys decreases, compared to the number available for scattering from the cold to the hot set. Ionized impurity scattering had a negligible effect on repopulation at 600 V/cm (1.87 Ω cm material).

Although the theoretical conductivity ratio versus E curves (Fig. 8) generally follow the experimental results, the theoretical curves for resistivities less than 214 Ω cm are about (5–10)% too high over most of the field range. At fields greater than 2000 V/cm this error can be attributed to the inexact theoretical fit to the 214 Ω cm conductivity ratio.[3] However, the disagreement between experiment and theory in the field range where the fit was excellent (200–1200 V/cm) remains to be accounted for. Several sources of error will be considered.

The first possibility we look at is our theoretical neglect of the increase in electron concentration with field, which apparently results from ionization of neutral donor sites (Sec. VIII). There will not be a direct effect on the conductivity ratio because both the ⟨111⟩ and ⟨100⟩ conductivities will increase with increasing concentration; however, there will be more e-e scattering than we have taken into account theoretically (it was assumed that the electron concentration remains at its equilibrium value n_0 independent of field). If there were a large amount of such ionization, the experimental curves should be below those determined theoretically because the increased concentration reduces repopulation. It is shown in Sec. VIII that it is unlikely for electron concentration to increase more than 30% for fields below 1200 V/cm. Our work, however, indicates that a much larger increase in electron concentration (approximately 180%) at high fields would be necessary to affect an agreement between experiment and theory.[24] Thus, this mechanism is probably not a major source of disagreement exhibited in Fig. 8.

Another source of error is that which results from our theoretical neglect of ionized impurity scattering anisotropy.[3] In n silicon the anisotropy ratio $\tau_\parallel/\tau_\perp$ is equal to roughly four,[29] so that for a ⟨100⟩ field, ionized impurity scattering in the hot valleys is stronger relative to that in the cold valleys, compared to the case of no anisotropy. It follows that if anisotropy were included in our ⟨100⟩ calculation, there might be a decrease in

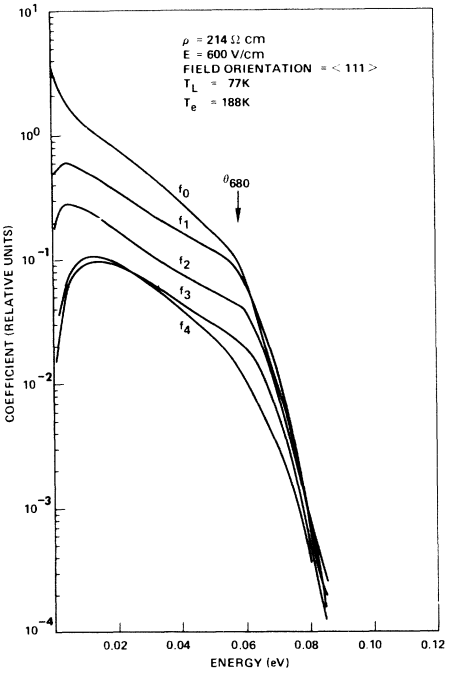

FIG. 11. First five Legendre coefficients of the distribution function vs energy for a ⟨111⟩ field of 600 V/cm and a resistivity of 214 Ω cm. The 680 K phonon energy is indicated by the arrow.

the electron temperature difference between hot and cold valleys. This would reduce repopulation, which in turn would reduce the theoretical conductivity ratio. However, at a ⟨100⟩ field of 600 V/cm for 1.87 Ω cm material, it was found that neglect of ionized impurity scattering had a negligible effect on repopulation. Thus, it seems unlikely that our neglect of ionized impurity anisotropy should be of great consequence.

Finally, we look at the role that might be played by intervalley scattering due to impurities. Both ionized and neutral impurities contribute mechanisms by which an electron can transfer valleys. For ionized impurities one transfer mechanism is a complex process in which an electron in a particular valley is captured at a donor site and later emitted into another valley.[30] This "capture and reemission" process can occur because a hydrogenlike donor-wave function is not associated with a particular valley, but with all six valleys. For neutral impurities the intervalley transfer occurs via an exchange scatter.[30] An incoming electron associated with a particular valley exchanges places with an electron bound to donor during a collision. The outgoing electron will, of course, be knocked randomly into a valley; hence, an intervalley transfer can occur. Intervalley transfer by ionized impurities can also occur by a direct elastic scatter caused by the large unshielded potential near the donor site. This rate has been determined for impurities in Ge.[31] The same formulation applied to Si shows that it is unimportant.[24]

There has apparently been no work reported on intervalley scattering by the capture and reemission or the exchange process in *n*-silicon. Even theoretical understanding of the recombination of an electron on an ionized donor is not completely understood.[32] Thus, we feel that the lack of accord between theory and experiment shown in Fig. 8 is most likely attributable to some form of intervalley impurity scattering.

VII. EFFECT OF *e-e* AND IMPURITY SCATTERING ON *f*

Figures 11–13 show the changes that occur in f for a ⟨111⟩ field of 600 V/cm as the concentration is increased from $2.25\times10^{13}\,\mathrm{cm}^{-3}$ (214 Ω cm) to $2\times10^{16}\,\mathrm{cm}^{-3}$ (0.049 Ω cm). It is evident that f becomes more Maxwellian and more isotropic ($f_0 \gg f_n$, $n>0$) as concentration increases. Intravalley ionized and neutral impurity scattering tend to reduce f to isotropic form, whereas e-e scattering works primarily to produce a more-Maxwellian f. At low energies for 0.049-Ω cm material, the coefficients f_2 to

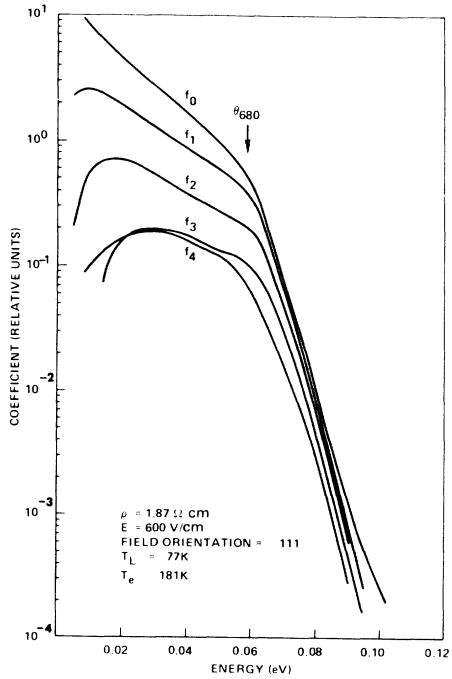

FIG. 12. First five legendre coefficients of the distribution function vs energy for a ⟨111⟩ field of 600 V/cm and a resistivity of 1.87 Ω cm. The 680 K phonon energy is indicated by the arrow.

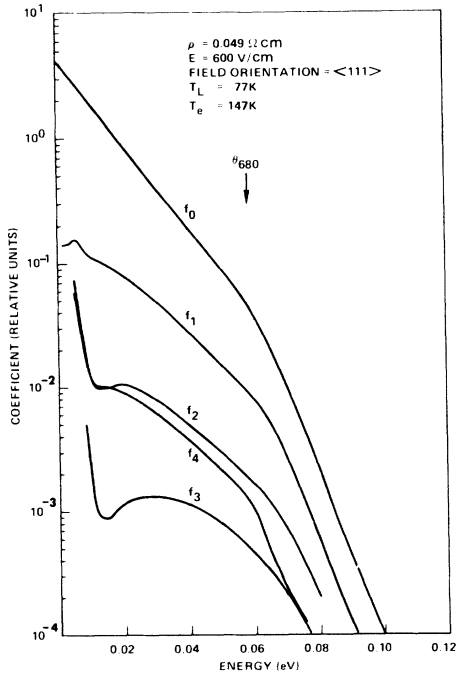

FIG. 13. First five Legendre coefficients of the distribution function vs energy for a ⟨111⟩ field of 600 V/cm and a resistivity of 0.049 Ω cm. The 680 K phonon energy is indicated by the arrow.

f_4 increase rapidly. This behavior, which departs considerably from that at other concentrtions, is due to the neglect of ionized impurity scattering at those energies. This clearly demonstrates its effect on distribution function isotropy.

In Figs. 14 and 15, we plot $T_{\rm loc}$ as a function of energy and concentration for two ⟨111⟩ fields. From these, one sees directly the manner in which e-e scattering smoothes "bumps" in f_0. It is interesting to note that the influence exerted by e-e scattering on f_0 in the high-energy tail is comparable to that at lower energies. One might intuitively expect that any effects from e-e scattering would decrease with electron energy since faster particles scatter less when the interaction potential is Coulomb repulsion. The reason for the significant e-e effect in the high-energy tail is that $(\partial f_0/\partial t)_{e-e}$, which determines the e-e scattering strength, is proportional at high energies to $[T_e/T_{\rm loc}(\epsilon)]^2$ [Eq. (21)]. Since in the tail of f, $T_{\rm loc}(\epsilon) \ll T_e$, $(\partial f_0/\partial t)_{e-e}$ is increased significantly there. In this manner, the e-e interaction becomes much stronger [through $(T_e/T_{\rm loc})^2$], depending upon the degree of distortion of f_0 from Maxwellian form; thus, e-e scattering has considerable effect on the high-energy tail of f because there is much distortion there.

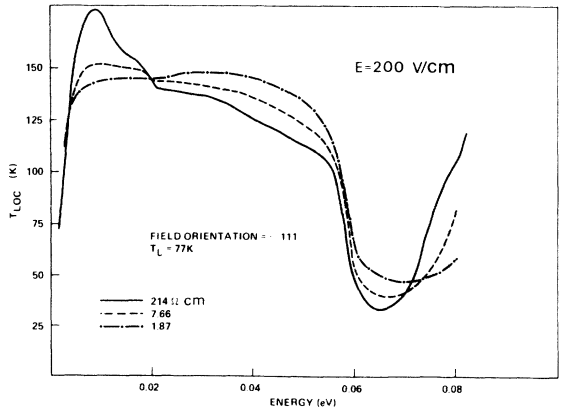

FIG. 14. Variation of $T_{\rm loc}$ as a function of energy at a ⟨111⟩ field of 200 V/cm.

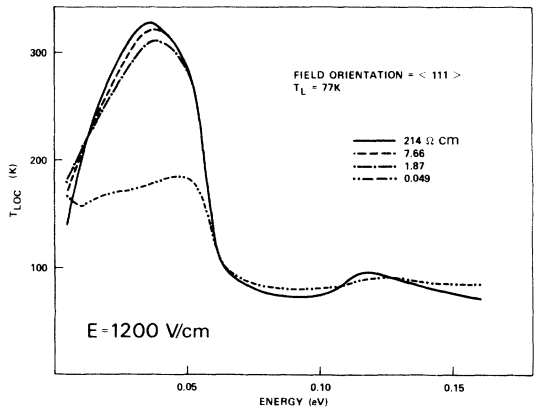

FIG. 15. Variation of $T_{\rm loc}$ as a function of energy at a ⟨111⟩ field of 1200 V/cm.

It would be interesting to determine that concentration at which f_0 can adequately be approximated by a simple-Maxwellian distribution at 77 K in n-Si. This is important because various values of concentrations have been used to justify this form. Our work shows that at a field of 600 V/cm, f_0 has not yet attained a Maxwellian form for n_0 as high as 2.3×10^{16} (Fig. 13). It does appear, however, that a good approximation to f_0 can be obtained for the 0.049 Ω cm material at fields as high as 1200 V/cm, (Fig. 15) using a Maxwellian distribution characterized by two temperatures, one for energies less than 680 K and one for energies more than 680 K. This approximation to f_0 for 1.87 Ω cm material ($n_0 = 1.3\times10^{15}$ cm^{-3}) at a lower field of 200 V/cm (Fig. 14) also appears to be good.

VIII. FIELD-DEPENDENT EMISSION

It has been assumed in the preceding analyses that during the application of high-field voltage

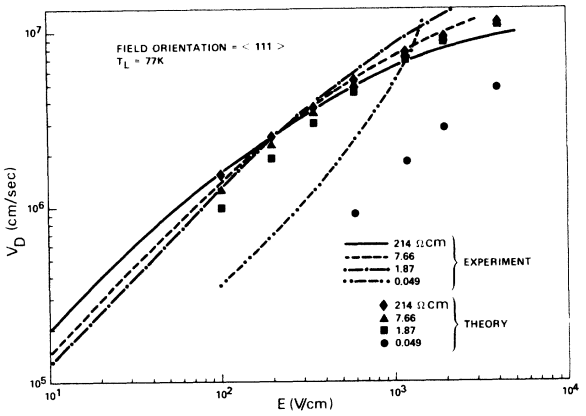

FIG. 16. Theoretical and experimentally inferred variation of drift velocity with field.

pulse, the free-electron concentration was equal to its thermal equilibrium value n_0. If this were the case, then electron drift velocity v_D could be inferred by dividing J by $n_0 e$. Comparisons between v_D determined in this manner and that obtained theoretically as a function of ⟨111⟩ field and resistivity is made in Fig. 16. One notes in this figure that at fields greater than 300 V/cm, v_D increases with decreasing resistivity (except for 0.049-Ω cm material). This behavior is clearly not acceptable physically because the addition of impurities to a pure specimen could only lower the mobility for a given field, hence v_D should decrease with impurity concentration for any given value of field (as shown by the theoretical results). It is unlikely that any appreciable errors have been introduced by an incorrect determination of n_0, because we have obtained good agreement between experimentally and theoretically determined resistivity at Ohmic fields. The experimental J-vs-E results of Asche *et al.*,[4] obtained using a different measurement technique (transmission line pulses), yielded v_D-vs-E curves with the same dependence on resistivity. (Their values of n_0 obtained from Hall measurements were used.)

Thus, it appears that in order to explain our experimentally inferred v_D-vs-E results we must assume that the electron concentration increases with field. This effect will be termed field-dependent emission. Field-dependent emission has been reported by Larrabee[33] (77 K) and Martini and McMath[34] (10 K) in p-Si, and by Kaiser and Wheatly[35] (20 K) in n-Si.

Presumably field-dependent emission occurs by either a phonon or Auger-assisted emission of an electron from a neutral (un-ionized) donor site.

To estimate the amount of field-dependent emission we note that at 1200 V/cm, the theoretical values of v_D for 214, 7.66, and 1.87 Ω cm coincide at the 214-Ω cm value. If we assume that the experimental values of the *actual* drift velocity also coincide at this field, then the deviations from this value indicated in Fig. 16 can be attributed directly to the increase in free carrier concentration. From Fig. 16 this gives a 30% and 10% increase in free-carrier concentration for 1.87- and 7.66-Ω cm material, respectively, at 1200 V/cm.

IX. ANALYSIS OF EXPERIMENTALLY DEDUCED RESULTS

The experimentally deduced repopulation as a function of field is shown in Fig. 17 along with the corresponding theoretically calculated results for 214-, 7.66-, 1.87-, and 0.049-Ω cm resistivities. The 214-Ω cm experimental and theoretical curves are in very good accord. Here, agreement is best at low fields where the assumption of an isotropic distribution function used in the scaling technique is most valid.[8] At higher fields the distribution becomes increasingly more distorted, causing an error in the experimentally deduced repopulation ratio of roughly 10% at 2000 V/cm. (In arriving at this error estimate, account has been taken of the overestimate of repopulation at higher fields shown in Fig. 8, which resulted from a less than perfect fit to the 214-Ω cm curve.)

For the rest of the resistivities the agreement is not as good. In every case the theoretical repopulation is larger in magnitude than the corresponding experimental values. This lack of agreement could be expected because the same behavior occurred in the comparison of experimental and theoretical conductivity ratios (Fig. 8). In fact, the difference between the experimental and theoretical curves in Fig. 8 can entirely explain the difference between the corresponding curves in Fig. 17.

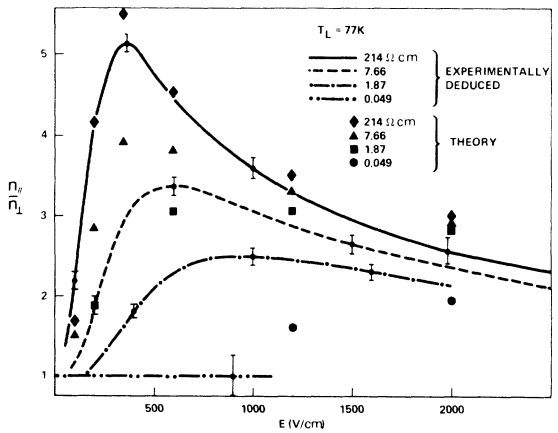

FIG. 17. Theoretical and experimentally deduced repopulation vs ⟨100⟩ field.

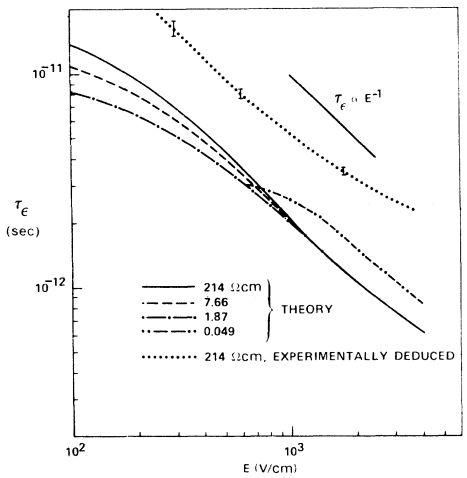

FIG. 18. Theoretical and experimentally deduced phenomenological energy relaxation time vs ⟨111⟩ field.

The theoretical energy relaxation time τ_ϵ, defined by the relation

$$\left\langle \frac{d\epsilon}{dt} \right\rangle = \frac{\langle \epsilon \rangle - \frac{3}{2} k_0 T_L}{\tau_\epsilon} ,$$

is shown in Fig. 18 as a function of field and concentration. Here $\langle d\epsilon/dt \rangle$ is the sum of the energy-loss contributions from acoustic and all intervalley phonons. The experimentally deduced phenomenological energy-relaxation time for 214-Ω cm material is shown for comparison. The experimental τ_ϵ is calculated using techniques described in Ref. 8. The agreement between the experimentally deduced and theoretical values of τ_ϵ for 214 Ω cm is not bad, considering the approximate nature of the phenomenological approach. The theoretical variation of τ_ϵ with resistivity seems physically consistent. At low fields there is a decrease in τ_ϵ with decreasing resistivity due to the filling of the tail with electrons, where intervalley phonons are able to relax away their energy. At high fields the 214-, 7.66-, and 1.87-Ω cm curves converge, indicating that impurity scattering and e-e scattering are no longer important. The shift of the 0.049-Ω cm resistivity curve in the direction of higher fields is another manifestation of the reduction of electron heating due to increased impurity scattering.

X. CONCLUSION

A comprehensive study of electron scattering in n-Si at 77 K, under the highly nonequilibrium conditions created by large applied electric fields has been presented. This study was based on a theoretical analysis of accurate J-vs-E measurements made on ⟨111⟩ and ⟨100⟩ crystallographically oriented samples with resistivities ranging from 0.049 to 214 Ω cm.

Theoretical calculations of the ⟨111⟩ and ⟨100⟩ conductivity ratio were performed using a numerical iterative technique which allows an "exact" solution to the Boltzmann transport equation. Electron-electron scattering was included using the Fokker-Plank formulation. The results showed that e-e scattering was primarily responsible for the decrease in conductivity ratio with increasing concentration through its effect on repopulation. Both intervalley and intravalley e-e scattering were important. Neutral impurity scattering was also shown to contribute to the reduction in ⟨100⟩ repopulation with increasing concentration at 600 V/cm, although ionized impurity scattering had negligible effect.

The field and concentration dependence of repopulation was deduced by a phenomenological scale change technique. The results were consistent with theoretical calculations.

The effect of e-e and impurity scattering on the nonequilibrium distribution function f was investigated by examining the concentration dependence of f at 600 V/cm.

Experimental v_D-vs-E curves obtained by dividing J by $n_0 e$, were found to be physically inconsistent at high concentrations. A field-dependent emission of electrons from neutral-donor sites to the conduction band was postulated to explain the inconsistencies.

APPENDIX

In order to carry out the indicated gradients in Eq. (17) it is best to rewrite it in tensor form as follows:

$$\frac{1}{A}\left(\frac{\partial f^{(i)}}{\partial t}\right) = -\sum_j \sum_m \sum_n \left[\frac{\partial}{\partial v_m} \left(2 f^{(i)}(\vec{v}) \frac{\partial}{\partial v_m} S^{(j)}(\vec{v}) \right) + \frac{1}{2} \frac{\partial}{\partial v_m} \frac{\partial}{\partial v_n} \times \left(f^{(i)}(\vec{v}) \frac{\partial}{\partial v_m} \frac{\partial}{\partial v_n} T^{(j)}(\vec{v}) \right) \right] . \tag{A1}$$

The summation above is over velocity components. Using the relations

$$\nabla^2 S^{(j)}(\vec{v}) = -4\pi f^{(j)}(\vec{v})$$

and

$$\nabla^2 T^{(j)}(\vec{v}) = 2 S^{(j)}(\vec{v}) ,$$

it is easily shown that Eq. (A1) becomes

$$\frac{\partial f^{(i)}}{\partial t} = A \sum_j \sum_m \sum_n \left[4\pi f^{(i)}(\vec{v}) f^{(j)}(\vec{v}) + \frac{1}{2} \left(\frac{\partial^2 f^{(i)}}{\partial v_m \partial v_n} \right) \left(\frac{\partial^2 T^{(j)}}{\partial v_m \partial v_n} \right) \right] . \tag{A2}$$

If f is replaced by the first term in its Legendre expansion, then according to the normalization convention in Ref. 3, this requires only the substitution

$$f(\vec{v}) = f_0(v)/\sqrt{2}$$

and

$$T(\vec{v}) = T_0(v)/\sqrt{2} \ .$$

Now, since $f_0^{(i)}$ and $T_0^{(j)}$ are only functions of the magnitude of velocity, Eq. (A2) can be simplified to

$$\frac{\sqrt{2}}{A}\left(\frac{\partial f_0^{(i)}}{\partial t}\right) = 4\pi f_0^{(i)}(v) f_0^{(j)}(v) + \frac{1}{v^2}\left(\frac{\partial T_0^{(j)}}{\partial v}\right)\left(\frac{\partial f_0^{(i)}}{\partial v}\right) + \frac{1}{2}\left(\frac{\partial^2 f_0^{(i)}}{\partial v^2}\right)\left(\frac{\partial^2 T_0^{(j)}}{\partial v^2}\right) ,$$

where use has been made of the relations

$$\frac{\partial^2 T_0^{(j)}}{\partial v_m \partial v_n} = \frac{\delta_{mn}}{v}\frac{\partial T_0^{(j)}}{\partial v} + \frac{v_m v_n}{v}\frac{\partial}{\partial v}\frac{1}{v}\frac{\partial T_0^{(j)}}{\partial v}$$

and

$$v_m v_n \frac{\partial}{\partial v_m}\frac{\partial}{\partial v_n} f_0^{(i)}(v) = v\frac{\partial}{\partial v^2} f_0^{(i)}(v) \ .$$

---

*Research supported by the National Science Foundation.

†Present address: Hughes Research Laboratories, Malibu, Calif.

[1]Preliminary results of this study are given in James G. Nash and James W. Holm-Kennedy, Appl. Phys. Lett. 27, 38 (1975).

[2]H. D. Rees, J. Phys. Chem. Solids 30, 643 (1969).

[3]James G. Nash and James W. Holm-Kennedy, Phys. Rev. B (to be published). The relevant "many valley" hot-electron hot-electron effects described in this paper were first identified by M. Shibuya, Phys. Rev. 99, 1189 (1955); W. Sasaki and M. Shibuya, J. Phys. Soc. Jpn. 11, 1202 (1956); and M. I. Nathan, Phys. Rev. 130, 2201 (1963).

[4]M. Asche, B. L. Boichenko, V. M. Bondar, and O. G. Sarbei, Phys. Status Solidi B 44, 173 (1971).

[5]V. Dienys and Z. Kancleris, Phys. Status Solidi B 67, 317 (1975).

[6]A. B. Davydov, Sov. Phys.-Semicond. 2, 1239 (1969). The sensitivity of β to electron concentration was the basis for probably the most rigorous "warm" electron treatment of e-e scattering to date. This was reported by A. Hasegawa and J. Yamashita, J. Phys. Soc. Jpn. 17, 1751 (1962). They used the Boltzmann-collision integral to describe the e-e interaction in their variational calculation of f for n-Ge at 77 K.

[7]P. Kastner, E. Roth, and K. Seegar, Z. Phys. 187, 359 (1972).

[8]J. W. Holm-Kennedy and K. S. Champlin, J. Appl. Phys. 43, 1878 (1972).

[9]M. H. Jorgenson, N. O. Gram, and N. I. Meyer, Solid State Commun. 10, 337 (1972).

[10]H. Heinrich and M. Kriechbaum, J. Phys. Chem. Solids 31, 927 (1970).

[11]B. L. Boichenko and M. Vasetskii, Fiz. Tverd. Tela 7, 2021 (1965) [Sov. Phys.-Solid State 7, 1631 (1966)].

[12]C. Canali, C. Jacoboni, F. Nava, G. Ottaviani, and A. Alberigi-Quaranta (unpublished).

[13]J. P. Nougier, M. Roland, and D. Gasquet, Phys. Rev. B 11, 1497 (1975).

[14]M. Asche, V. M. Bondar, and O. G. Sarbei, Phys. Status Solidi 31, K143 (1969).

[15]C. Irvin, Bell Syst. Tech. J. 41, 387 (1962).

[16]D. Long and J. Meyers, Phys. Rev. 115, 1107 (1959).

[17]W. Kohn and J. M. Luttinger, Phys. Rev. 98, 915 (1955).

[18]D. Long and J. Meyers, Phys. Rev. 115, 119 (1959).

[19]The corresponding J-vs-E curves are given in James G. Nash and James W. Holm-Kennedy, Appl. Phys. Lett. 24, 139 (1974).

[20]These curves differ slightly from those reported in Ref. 19, in which $\tau_{\parallel}/\tau_{\perp} = 0.67$ for acoustic scattering was used. Here we have used $\tau_{\parallel}/\tau_{\perp} = 1.0$.

[21]H. D. Rees, J. Phys. Chem Solids 30, 643 (1969).

[22]T. J. M. Boyd and J. J. Sanderson, *Plasma Dynamics* (Barnes & Noble, New York, 1969), p. 285.

[23]A. N. Kaufman, in *The Theory of Neutral and Ionized Gases*, edited by C. DeWitt and J. F. Detoeuf (Wiley, New York, 1960) (cited in Ref. 22).

[24]James G. Nash, Ph.D. dissertation (University of California, Los Angeles, 1974) (unpublished).

[25]I. M. Dykman and P. M. Tomchuk, Sov. Phys.-Solid State 7, 224 (1965).

[26]C. Erginsoy, Phys. Rev. 79, 1013 (1950).

[27]Harvey Brooks, in *Advances in Electronics and Electron Physics*, edited by L. Marton (Academic, New York, 1955), p. 161.

[28]Intravalley e-e scattering refers to collisions between electrons within a set of cold valleys or within a set of hot valleys, whereas intervalley e-e scattering refers to collisions between electrons in the cold set of valleys and electrons in the hot set of valleys. Any large-angle collisions that would allow an electron to transfer between hot and cold sets of valleys is assumed unimportant.

[29]F. S. Ham, Phys. Rev. 100, 1251 (1955).

[30]G. Weinreich, T. M. Sanders, and H. G. White, Phys. Rev. 114, 33 (1959); and B. Tell and G. Weinreich, *ibid.* 143, 584 (1966).

[31]P. J. Price and R. L. Hartman, J. Phys. Chem. Solids 25, 567 (1964).

[32]P. Norton, T. Braggins, and H. Levinstein, Phys. Rev. Lett. 30, 488 (1973).

[33]R. D. Larrabee, Phys. Rev. 116 300 (1959).

[34]M. Martini and T. A. McMath, Solid State Electron 16, 129 (1973).

[35]W. Kaiser and G. H. Wheatly, Phys. Rev. Lett. 3, 334 (1959).